THE ASTROPHYSICAL JOURNAL, 482:L175–L178, 1997 June 20

FIRST *HUBBLE SPACE TELESCOPE* OBSERVATIONS OF MIRA AB WIND-ACCRETING BINARY SYSTEM

MARGARITA KAROVSKA
Harvard-Smithsonian Center for Astrophysics, 60 Garden Street, Cambridge, MA 02138
WARREN HACK
Space Telescope Science Institute, 3700 San Martin Drive, Baltimore, MD 21218
JOHN RAYMOND
Harvard-Smithsonian Center for Astrophysics, 60 Garden Street, Cambridge, MA 02138
AND
EDWARD GUINAN
Villanova University, Villanova, PA 19085
Received 1997 February 5; accepted 1997 April 4

ABSTRACT

The Mira AB system belongs to a class of detached binaries in which a compact object accretes mass from the wind of a cool giant or supergiant. This system provides a unique laboratory for detailed study of the characteristics of the wind accretion processes because it can be spatially resolved with the *Hubble Space Telescope* (*HST*) and the components can be studied individually at UV and optical wavelengths.

We resolved the components of this binary using *HST* Faint Object Camera (FOC) images and obtained spectra of each component separately for the first time. The multiwavelength FOC images combined with the spectra provide a unique perspective on this accreting system and its components at wavelengths ranging from 150 to 550 nm. We determined the spectral energy distribution of each component unambiguously at UV and optical wavelengths and obtained the first high spatial resolution images of Mira A and Mira B at UV wavelengths. We detected significant asymmetries in the giant's atmosphere and found evidence for possible interaction with its companion.

Subject headings: accretion, accretion disks — binaries: close — stars: individual (*o* Ceti)

1. INTRODUCTION

Mira AB is the nearest binary system (at distance of 77 pc; Jenkins 1952) composed of a Mira-type variable star (*o* Ceti [Mira]) and an accreting companion (VZ Ceti [Mira B]). The system primary is a pulsating, cool giant (M2–M7 III) with a diameter of several hundred solar radii and a mass comparable to that of our Sun. The brightness of this star varies over 7 magnitudes between its minimum and maximum, over a period of 332 days. Mira A is losing mass at the rate of about $1 \times 10^{-7} M_{\odot}\ \mathrm{yr}^{-1}$ (e.g., Bowers & Knapp 1988) via a slow wind as it approaches the final stages of its evolution toward a planetary nebula. The companion, Mira B (VZ Ceti), was discovered by Joy (1926) during spectroscopic observations at Mira A minimum. It is possibly a white dwarf embedded in an accretion disk of variable luminosity.

This detached binary system belongs to a very important class of accreting systems where the primary does not fill its Roche surface, and the mass transfer occurs by wind interaction rather than by tidal interaction. The amount of material the accreting star can capture from the surrounding medium depends on the properties of the wind (density and velocity), the properties of the binary (orbital period and separation), and the dynamics of the flow. Mira AB is one of the few accreting systems in which most of the important parameters needed for accretion rate and luminosity calculations (e.g., Livio 1988) can be determined unambiguously from the observations, because the system and/or its components can be resolved and studied in detail at wavelengths ranging from the X-ray to the radio region.

The *Hubble Space Telescope* (*HST*) provides an exceptional opportunity for exploring the characteristics of this system because important spectral diagnostics of the accretion processes occur at UV wavelengths. In addition to the possibility of observing Mira B uncontaminated by Mira A (especially in the near-UV and optical), the angular resolution of the COSTAR-corrected optics of the *HST* provides a unique opportunity for high spatial resolution imaging of Mira A. The Faint Object Camera (FOC) f/96 has a point-spread function (PSF) with FWHM of 45 mas at 550 nm, decreasing to about 30 mas in the UV (FOC Instrument Handbook, Version 7.0 [Nota et al. 1996]).

In this Letter we present the results of the first *HST* observations of the Mira AB system using the FOC camera and the objective prisms; the observations were obtained when Mira A was near minimum brightness (J. Mattei, private communication), at phase 0.6 of its pulsation cycle.

2. *HST* OBSERVATIONS

We carried out *HST* observations using the FOC f/96 camera and objective prisms on 1995 December 11. FOC images were taken using the small 256×256 pixel format, with pixel sizes of 14.35 mas $\times$ 14.35 mas, which required an interactive acquisition in order to ensure that the target fell inside the $3\farcs5 \times 3\farcs5$ field of view. The images we recorded using a set of medium- and narrow-bandpass spectral filters (see Table 1) and neutral density filters (from 2 to 6 ND). Each exposure was 300 s long. These filters and the exposure times were chosen based on our understanding of the source fluxes derived from *IUE* and optical spectra of Mira AB at Mira A minimum light. Particular care was taken to ensure that both Mira A and Mira B were photometric in each image, since both components of the system are known to be variable. Although Mira A variability at optical wavelengths is well studied and reasonable predictions of its brightness can be

TABLE 1

SPECTRAL FILTERS

Filter	Central Wavelength (nm)	Bandpass (nm)
F152M.....	150.0	18.4
F278M.....	280.0	31.6
F307M.....	308.0	32.8
F346M.....	348.0	43.4
F410M.....	410.0	19.4
F470M.....	471.0	21.2
F501N	501.0	7.4
F550M.....	546.0	18.8

made based on its pulsation cycle, its variability in the UV (especially the Mg II [280 nm] $h + k$ lines) and its brightness in different spectral regions is difficult to predict. In addition, the variability of Mira B is not understood (see Joy 1954; Warner 1972; Yamashita & Maehara 1977; Reimers & Cassatella 1985). The choice of the short exposure times and the neutral density filters reflects our cautious and conservative approach to these initial observations, especially in the UV where the stars have not been imaged before. This format maintained linearity for point sources with peak count rates up to ≈5 counts s^{-1} $pixel^{-1}$. The FOC images gave us an overall view of this system in many different wavelengths, sometimes at the expense of the signal-to-noise ratio (S/N). The S/N varies from image to image; for example, the F501N and F505M images have S/N in the peak of about 15 and 30, respectively, while in some images (e.g., of Mira A at wavelengths lower than 300 nm) the S/N is not sufficient for detailed analysis.

Objective-prism images, taken with PRISM1 + F140W (far-UV objective prism; FUVOP) and PRISM2 + F175W (near-UV objective prism; NUVOP), provided low-resolution spectroscopy of both components, separated from each other for the first time ever. In order to separate the two sources with the objective-prism spectra, we planned the observations for a time when they would be separated by at least 0.″25 in the image's x-direction, since the FOC PSF still has detectable wings out to a radius of 0.″5 for bright sources. The observations had an orientation such that the angle between the image's y-axis and north was 22° with a separation of nearly 0.″6 between Mira A and Mira B. The 300 s exposures were taken using the 256 × 1024 pixel format in order to cover the entire spectrum of the targets. These observations gave a S/N ranging from ≈5 at 165 nm to ≈15 at 300 nm. For wavelengths longer than 300 nm, the light from the primary became slightly nonlinear but still had a peak count rate of less than 1 count s^{-1} $pixel^{-1}$ for the PRISM2 image. This level of nonlinearity in the FOC data only introduced an additional error in the wide-band spectrophotometry of ≈0.1 mag.

3. DATA ANALYSIS

The observations were flat-fielded and geometrically corrected using the standard FOC pipeline calibrations described in detail in Nota et al. (1996). The dispersed images taken with the objective prisms are aligned with the visible wavelengths on the lower end and the UV wavelengths at the upper end. The FUVOP image has a resolution of 50 nm $pixel^{-1}$ at 500 nm, which increased to 0.2 nm $pixel^{-1}$ at 130 nm with the spectra extending across 180 pixels. The NUVOP image had a resolution of 4 nm $pixel^{-1}$ at 500 nm and 0.05 nm $pixel^{-1}$ at 170 nm, covering over 750 pixels. A 7 pixel (0.″1) wide region centered on the peak of each spectrum was extracted and summed to provide the raw spectrum. The raw spectra were then converted from counts per pixel to counts per angstrom by applying the latest dispersion relation for each prism as given in the FOC Instrument Handbook (Nota et al. 1996). The zero point for the conversion was set based on the position of each star in the F550M image. Flux-calibrating the spectrum required some knowledge of the percentage of total flux from the source that was contained in the spectrum to recover all the flux from the source. This percentage was based on the width of the extraction used for the spectrum, which was 7 pixels for Mira A and Mira B. An empirical relationship for this percentage had been determined using spectrophotometric standards and reported in the FOC Instrument Handbook (Nota et al. 1996), and served as the initial estimate for our reductions. This value was further refined using the average flux rates seen in the direct images taken through the F253M and F410M filters, with a best fit resulting in a value of 0.67 for the NUVOP spectrum. This ensured that the spectra derived from the objective-prism observations had fluxes consistent with those derived from the direct images.

Differences in the detector sensitivity between the various imaging formats have been noted for the FOC (Nota et al. 1996). This was investigated for the objective-prism images, since they were taken in a format whose sensitivity had not been fully calibrated. By analyzing NUVOP observations of a spectrophotometric standard taken as part of the normal calibration program for the FOC, it was determined that the format used for the objective-prism observations had a sensitivity that was 90% of the standard throughput. This correction was then applied to the extracted spectrum in the final flux calibration, when the filter transmissions and instrument sensitivities were divided out to produce the fully calibrated spectra.

The synthetic photometry package in the Space Telescope Science Data Analysis System (STSDAS), *synphot*, was used to calculate observed magnitudes given the calibrated objective-prism spectra. Observed instrumental magnitudes were calculated for the filters used in the direct images allowing for direct comparison between the two sets of data. The accuracy of the calculated V magnitude may be affected by the fact that the NUVOP spectrum in the region from 500 to 600 nm is not as well calibrated as at shorter wavelengths. Photometry of the direct images, on the other hand, was done using core aperture photometry with 5.5 pixel radius apertures and a background annulus 6–12 pixels from the core. These apertures were chosen to encompass the entire disk of the primary so that it could be treated as a point source in the analysis with minimal impact on the photometry. Using the encircled energies provided in the FOC Instrument Handbook (Nota et al. 1996), an aperture-corrected total count rate was derived for each observation. This count rate was then divided by the filter throughputs as well as format and detector sensitivities (as provided in the image headers) to produce an average flux, which was then converted to an observed magnitude. In general, the photometry derived from the direct images and the objective-prism spectra has errors of ≈0.1 mag, which was low enough not to influence the results from our analysis.

The FOC images where both components were detected simultaneously with sufficiently high S/N provide an exceptional opportunity for high-resolution imaging using deconvolution techniques. Since Mira B is unresolved by the *HST*, its images can be used as PSFs for deconvolution of Mira A images taken under identical observing conditions. Mira A images were deconvolved with the corresponding Mira B images as PSFs using the Richardson-Lucy deconvolution algorithm (Richardson 1972; Lucy 1974). For comparison, we

also deconvolved Mira AB images using PSFs from the *HST* library of FOC PSFs taken using the same filters.

We measured the angular size of Mira A by fitting an elliptical Gaussian model of the brightness distribution on the disk to the reconstructed images. As a result, the angular sizes and the position angles of the major axes as well as the ratios of the minor to the major axes were estimated. Details of the fitting process including results obtained using other than Gaussian models of brightness distribution will be given elsewhere.

4. RESULTS

4.1. *Imaging of the Mira AB System*

The direct images taken in the near-UV and the optical with the FOC provided the most accurate positional data for the secondary ever recorded. Both components of the system were simultaneously detected in the FOC images recorded at wavelengths from 278 to 550 nm. Mira B was also detected in the FOC images recorded at shorter wavelengths down to 152 nm. In Figure 1*a* (Plate L10) we show, as an example, the image of the system recorded using the F501N filter, where both components have similar brightness. Using the set of images where both components were detected, we determined the separation and the position angle of Mira B relative to Mira A by calculating the centroids of stellar images in each FOC image, and then averaging the results for the set. This approach resulted in measurements of the separation and the position angle of Mira B with an unprecedented precision: a separation of $0''.578 \pm 0''.002$ and a position angle of $108°.3 \pm 0°.1$. This measurement is in agreement with the previous speckle measurements of about $0''.6$ (within the error bars) (Karovska, Nisenson, & Beletic 1993), and follows the same trend of slowly decreasing apparent separation and position angle.

Since the angular distance between the components of the system is changing slowly, it will continue to be large enough for precise *HST* measurements of the separation and the position angle of Mira B to be taken in the near future. Further measurements will constrain the orbital parameters and finally allow an improvement of the orbit. This improved orbital solution can be used to derive the relative orbital velocity of Mira B and the major axis of the orbit, which, in addition to the total accretion luminosity, are critical parameters for validating the accretion models.

4.2. *Spectral Energy Distribution of Mira A and Mira B*

The FOC images and the near-ultraviolet (NUV) and far-ultraviolet (FUV) objective-prism spectra of Mira AB provided the first detailed information on the continuum and line emission from each component of the system. Furthermore, they provided the first view of the spectra of each component in the spectral region longward from 320 nm. Figure 2 shows the NUV objective-prism spectra of Mira A and Mira B. In addition to separating the continuum emission from each source, these spectra allowed us to unambiguously determine which lines originated in Mira A and which from Mira B. The emission from Mira A at wavelengths shorter than about 170 nm is very faint, and therefore it was not detected in the FUV spectrum.

Using the FOC images and the spectra, we made the first unambiguous measurements of the brightness of Mira A and Mira B at UV and optical wavelengths (Table 2). Previous attempts to determine the Mira B luminosity in the NUV and optical wavelengths had limited success because the emission in this spectral region is dominated by Mira A.

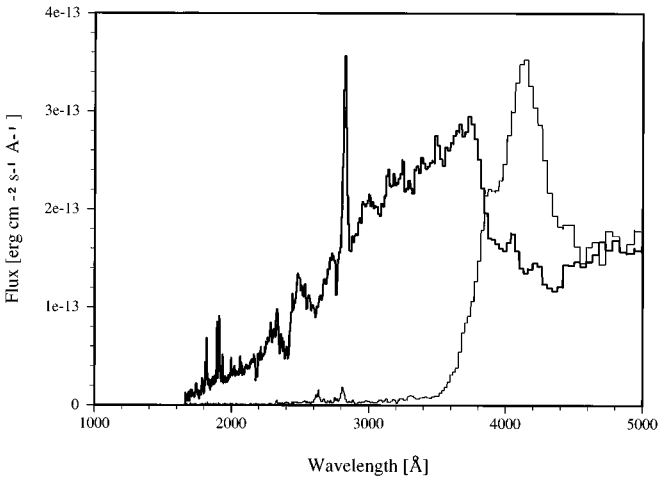

FIG. 2.—Near-UV objective-prism spectra of Mira A and Mira B: *thin line*, Mira A spectrum; *thick line*, Mira B spectrum.

The objective-prism spectra of Mira B detected a large number of lines. In addition to the prominent Mg II $h + k$ emission feature at 280 nm, we resolved several emission lines, including C III 191 nm, Si III 189 nm, Si II 182 nm, Fe II 179 nm, and N III 175 nm. We also detected several Fe absorption lines, including the Fe II (1) 262 nm multiplet, similar to the absorption features detected in the *IUE* observations (Reimers & Cassatella 1985).

Several strong emission features were detected in the Mira A NUV spectrum (Fig. 3). The Mg II $h + k$ emission in the Mira A spectrum was seen for the first time uncontaminated by the Mg II emission from Mira B. Another prominent emission feature in this spectrum was identified as the Fe II (1) 262 nm multiplet. This feature is seen in absorption in the Mira B spectrum in Figure 2. In fact, single Miras do not have strong emission at 262 nm at minimum light, and this emission feature has not been detected in the *IUE* spectra of other Miras recorded at the minimum light phase (Kafatos et al. 1980). Therefore, it could be formed in the Mira A atmosphere as a result of heating or fluorescence effects from Mira B.

4.3. *Asymmetries in the Mira A Atmosphere*

The high angular resolution of the COSTAR-corrected FOC f/96 camera and the small pixel size provided an opportunity for exploring the Mira A atmosphere at spatial scales as small as 30 mas. The FOC images resolved Mira A at several optical wavelengths (F410M, F470M, F501N, F550M) and, for

TABLE 2

PHOTOMETRY OF MIRA A AND MIRA B

FILTER	IMAGE PHOTOMETRY		PRISM2 PHOTOMETRY	
	m(B)	m(A)	m(B)	m(A)
F152M + F175W.....	13.27[a]	...	(14.47)[b]	...
F278M + F275W + F4ND + F1ND...	10.94	15.17	10.91	14.68
F307M + F275W + F4ND + F1ND...	10.68	14.84	10.74	14.88
F346M + F6ND + F1ND.....	10.23	12.83	10.59	13.27
F410M + F6ND + F1ND.....	11.32	9.96	11.14	10.37
F470M + F6ND.....	11.33	11.17	11.10	11.07
F501N + F4ND + F1ND.....	11.30	11.16	11.06	10.76
F550M + F6ND.....	11.32	9.35	11.2	9.69

[a] Typical errors are ±0.15 mag.

[b] This magnitude does not include the full wavelength range for the filters used, and therefore underrepresents the true magnitude.

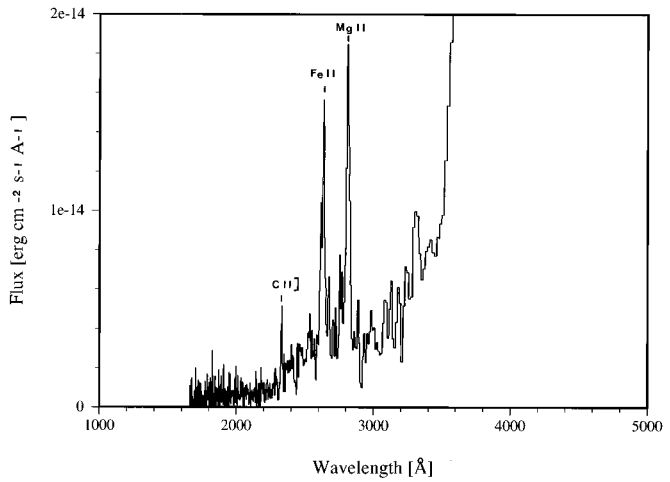

FIG. 3.—Near-UV objective-prism spectrum of Mira A showing several emission lines in the region between 200 and 360 nm.

the first time, one in the UV (F346M). The measured angular size varies as a function of wavelength. For example, the FWHM of a best-fit Gaussian to the deconvolved images varies from 35 mas at 346 nm to 56 mas at 501 nm. These size variations can be interpreted in terms of optical depth or opacity variations, possibly due to the effects of pulsation on the structure of the extended atmosphere. The large size measured at 501 nm is in agreement with the ground-based observations, showing that diameters measured in the center of the TiO band can be as much as twice as large as diameters measured at other wavelengths (Bonneau et al. 1982). This image is the only one recorded using a narrowband filter centered in the trough of one of the strong TiO absorption bands, and we are probably imaging the upper layers of the atmosphere of Mira A where the opacity of the TiO molecules is higher.

We detected asymmetries in the direct FOC images of Mira A. These asymmetries are clearly visible in the FOC images of Mira A, deconvolved using the images of the companion as point sources. The deconvolved images of Mira A show an asymmetry in the Mira A extended atmosphere in the south-east direction. This asymmetry is especially prominent in the F501N image. Figure 1*b* shows the F501N image of the system deconvolved using the image of Mira B as a PSF. Figure 1*c* shows the Mira A image from Figure 1*b* after being magnified 5 times using a bicubic spline interpolation for visualization purposes. The apparent size of the major axis of the dominant asymmetry as measured using elliptical Gaussian fitting to the deconvolved images is 56 ± 1 mas, with a position angle of $175° \pm 2°$. The estimated ratio between the minor and the major axis of the asymmetry is 0.2. Similar results were obtained using the PSFs from the FOC PSF library. This asymmetry is similar to the asymmetries previously detected using interferometry (e.g., Karovska et al. 1991; Haniff et al. 1992). The asymmetry in the Mira A image could be due to unresolved bright spots on the surface of the star or in the extended atmosphere. It could also be an indication of non-radial pulsation of the Mira A atmosphere, resulting in geometrical asymmetries and/or in temperature and density nonuniformities.

Another asymmetric feature was detected in the Mira A image recorded using the F346M filter, at the Balmer jump region. This feature is located in the vicinity of Mira A and extends toward the companion, and could be a result of Mira A's interaction with Mira B. Similar low-intensity structures were seen at that location at other wavelengths; however, their presence needs to be confirmed by further imaging with a higher signal-to-noise ratio. If the feature in the F346 image is associated with the Balmer continuum emission, it could be a denser region in the wind caused by Mira B's gravity, and it is probably photoionized by Mira B.

5. CONCLUSION

This is the first case of a wind-accreting system that has been spatially resolved with the *HST*, and the spectral energy distribution of its components has been determined unambiguously at UV and optical wavelengths. The main results of this study of the Mira AB system are the following:

1. First observation of the spectral energy distribution of Mira B and Mira B uncontaminated by each other, especially in the region of the Balmer jump.
2. First direct images of Mira A and Mira B in the UV.
3. Asymmetries in the Mira A atmosphere: a substantial elongation with a major axis at P.A. 175°, and an asymmetric feature extending toward the companion—possible evidence for interaction of the atmosphere or wind of Mira A with Mira B.

A further, detailed study of the characteristics of the accretion processes in this system (with an emphasis on their accretion luminosity) is extremely important for understanding accretion processes in a wide range of wind-accreting binaries, which cannot be as easily spatially resolved as Mira AB. The follow-up observations of the Mira AB system at selected wavelengths will also provide a basis to further explore the origin of the significant asymmetries in the Mira A atmosphere, especially possible signatures of interaction with Mira B. Finally, we hope that future observations of the system will allow improvement of the orbital solution parameters needed for validation of wind accretion models.

We are grateful to the members of the Space Telescope Science Institute (STScI) and particularly the FOC group for their help and support in implementing the *HST* observations. We wish to thank Janet Mattei for providing the AAVSO light curve of Mira A and calculation of the pulsation cycle phases, and Scott Kenyon for helpful suggestions and discussions. This work was supported in part by STScI grant GO-5822.01-94A to the Smithsonian Astrophysical Observatory.

REFERENCES

Bonneau, D., Foy, R., Blazit, A., & Labeyrie, A. 1982, A&A, 106, 235
Bowers, P. F., & Knapp, G. R. 1988, ApJ, 332, 299
Haniff, C. A., Ghez, A. M., Gorham, P. W., Kulkarni, S. R., Matthews, K., & Nagebauer, G. 1992, AJ, 103, 5, 1667
Jenkins, L. F. 1952, General Catalogue of Stellar Parallaxes (New Haven: Yale Univ. Obs.)
Joy, A. H. 1926, ApJ, 63, 333
———. 1954, ApJS, 1, 39
Kafatos, M., Michalitsianos, A. G., & Hobbs, R. W. 1980, A&A, 92, 320
Karovska, M., Nisenson, P., & Beletic, J. 1993, ApJ, 402, 311
Karovska, M., Nisenson, P., Papaliolios, C., & Boyle, R. B., 1991, ApJ, 374, L51
Livio, M. 1988, in IAU Colloq. 103, The Symbiotic Phenomenon, ed. J. Mikolajewska, M. Friedjung, S. J. Kenyon, & R. Viotti (Dordrecht: Kluwer), 149
Lucy, L. B. 1974, AJ, 79, 6, 745
Nota, A., Jedrzejewski, R., Voit, M., & Hack, W. 1996, FOC Instrument Handbook Version 7.0 (Baltimore: STScI)
Reimers, D., & Cassatella, A. 1985, ApJ, 297, 275
Richardson, W. H. 1972, J. Opt. Soc. Am., 62, 1, 55
Warner, B. 1972, MNRAS, 159, 95
Yamashita, Y., & Maehara, H. 1977, PASJ, 30, 409

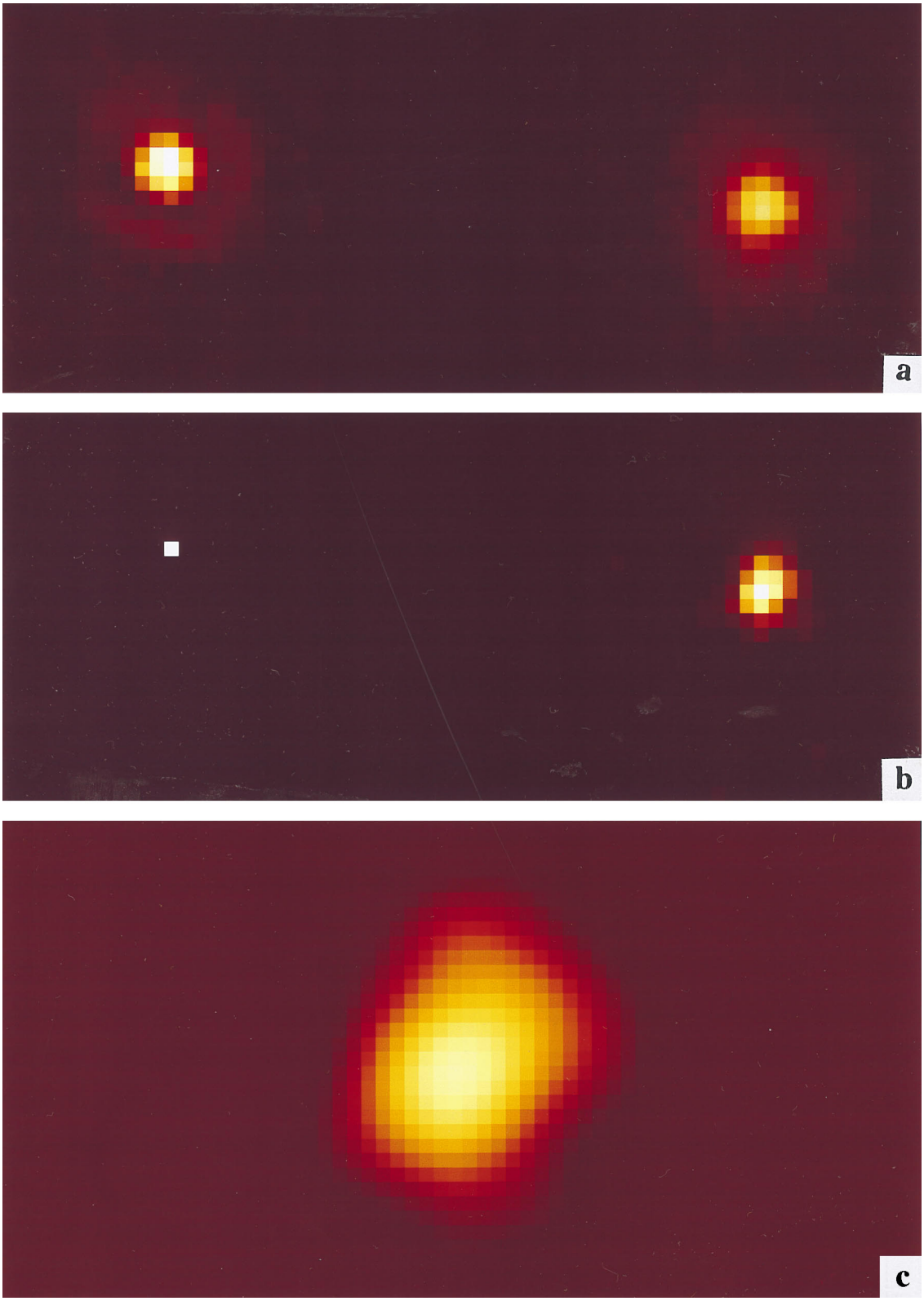

FIG. 1.—FOC images of Mira A (*right*) and Mira B (*left*) in the F501N filter, 0.58 arcseconds apart: (*a*) original data; (*b*) deconvolved images using Mira B as a PSF; (*c*) deconvolved image of Mira A, magnified 5 times using bicubic spline interpolation, showing the asymmetry in the Mira A atmosphere. North is 22° to the right from the vertical, and east is to the left.

KAROVSKA et al. (see 482, L177)